Thin embankments on soft soil reinforced with rigid inclusions: rolling load tests

Thierry Dubreucq[1], Luc Thorel[1], Alexandre Jagu[1], Stéphane Lerat[1], Alain Neel[1], Patrick Gaudicheau[1], Philippe Audrain[1]
[1] *Université Gustave Eiffel, Laboratoire Centrifugeuse Géotechnique, Nantes, France,*
thierry.dubreucq@univ-eiffel.fr

ABSTRACT: The effect of rolling loads on a thin granular platform, founded on soft soil reinforced with rigid inclusions, was studied using physical models reduced to 1/10th scale and centrifuged at 10×g, in 2D, a first step in the understanding of load transfer mechanisms, and then in 3D. Some test results are presented here. These physical models consist of a sand platform, possibly reinforced with a geogrid, a similar loose soil made of expanded polystyrene, and regularly spaced vertical metal inclusions. The coverage ratio of the inclusions is 10% in 2D and 4.52% in 3D. The assembly is placed in a rigid container with a transparent face in order to analyze the images of the rolling load and deduce the internal deformations. Traffic modeling is performed using a roller of variable length. One way rolling or two-ways rolling simulates linear traffic. The specific evolution of load transfer to the inclusion heads via the platform is shown. The arching and confinement effects of the geogrid in the platform are quantified using a tactile pad placed on the inclusion heads.

ABBREVIATIONS/NOTATIONS

G/R	: go and return of the rolling load
GGR	: fiberglass geogrid
LTP	: load transfer platform
RI	: rigid inclusion
E,M,V	: cylindrical instrumented inclusions
∅	: diameter of the RI in 3D [m]
a	: thickness of the RI in 2D [m]
d	: wheel and RI centre distance [m]
d_{50}	: median sand diameter [m]
E_{poly}	: elastic modulus of polystyrene [Pa]
E_Q	: load transfer efficiency on RIs [-]
E_u	: undrained soft soil modulus [Pa]
g	: earth acceleration, 9.81 m/s² [-]
H_{LTP}	: thickness of the LTP [m]
I_d	: sand density index [-]
J_{GGR}	: secant stiffness of the GGR [N/m]
l	: wheel width [m]
L	: roller length [m]
m	: wheel mass [kg]
M	: roller mass [kg]
N_g	: number of g applied to the model
Q	: rolling load weight [N]
Q_p	: vertical force at the head of the RI [N]
q_{LTP}	: constraint at the base of the LTP, [Pa]
Q_{sand}	: weight of the sand above a RI [N]
D	: diameter of the rolling load [m]
s	: RI centre distance, mesh width [m]
W_{LTP}	: weight of the LTP in a grid [N]
α	: RI coverage rate [-]
ϕ'_{sand}	: friction angle of Fontainebleau sand [°]
ρ_d	: dry bulk density of sand in the LTP [kg/m³]
ε_{GGR}	: local relative elongation of the GGR
$\sigma_{v(RI)}$	: vertical stress at the head of a RI [N/m²]
$\sigma_{v(poly)}$	: vertical stress on soft soil [N/m²]

1 INTRODUCTION

The improvement of soft soils using rigid vertical inclusions (RI) is now a widely used technique (Thorel et al., 2007; ASIRI, 2013; van Eekelen and Han, 2020). As part of the ASIRI+ project (Improvement and Reinforcement of Soils by RIgide Inclusions) launched in 2019 (Briançon et al., 2021), new researches have been explored, in particular that of rolling loads applied to thin granular load transfer platform (LTP), a case that had received little attention in previous studies (Lukiantchuki et al., 2018). Previous efforts have mainly focused on cyclic vertical loading tests carried out on 1×g laboratory-scale models (Liu et al., 2025; Wu et al., 2024).

After a series of two-dimensional (2D) centrifuge models using a heavy roller and plane rigid inclusions (RIs) (Dubreucq and Thorel, 2025), the research now focuses on the three-dimensional (3D) modeling of the behavior of a thin sandy layer, placed on a soft soil (a geofoam layer) reinforced by cylindrical inclusions, and subjected to a rigid wheel or roller simulating traffic. Modeling devices and a few test results in 2D and 3D are presented and compared in this article.

2 EXPERIMENTAL DESIGN

2.1 Experimental program

The 1/10th scale model includes (figure 1): a sandy load transfer platform (LTP) with H_{PTC} thickness; a possible stiffness geogrid (GGR); cylindrical RIs(3D) forming a square-mesh network, or plane RIs(2D) in the form of rigid vertical plates evenly spaced. Linear traffic is simulated with a heavy roller or a heavy wheel. Their diameter D is identical. The roller is spinning (2D effect), and the wheel is not wide (3D effect). A thin and flexible surface covers top of the LTP.

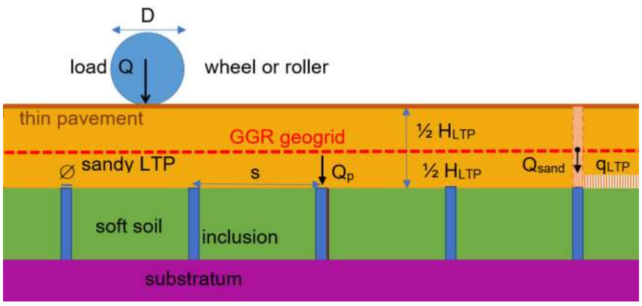

Figure 1. Scheme of physical models (2D or 3D RIs)

The model is placed in a container (80 cm long, 25 cm wide, 44 cm high) with a transparent face to allow the analysis of the images of the rolling load thanks to an on-board camera and a lighting (figure 2). The container is 80 cm long and 25 cm wide. The devices for loading and taking 2D and 3D images are identical (Dubreucq et al. 2022).

The model is subjected to centrifugal acceleration $N_g \times g$ = 10 × 9.81 m/s² applied to the base of the rolling load. The scale model is designed according to the scaling laws of physical modelling (Tables 1 and 2, Garnier et al., 2001).

During centrifuging, the stresses in the LTP model are identical to those in the prototype LTP in order to reproduce identical internal frictions.

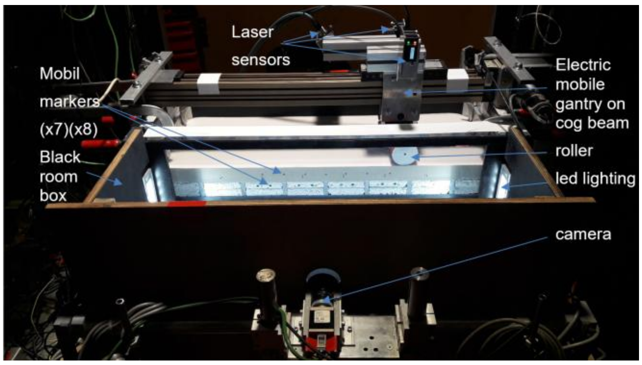

Figure 2. Rolling device (on 2D or 3D RIs) in the transparent face container, imaging device

The rolling load at the serviceability limit state is deduced from static loading tests carried out on 2D strip footings (Dubreucq et al., 2022).

The coverage rates α of 2D and 3D RIs are equal to 10% and 4.52% respectively.

Table 1. 2D RIs and scale factors at $N_g \times g$ =10×g.

parameters	unit	prototype		model	
H_{LTP}	cm	1	40	$1/N_g$	4
a	cm	1	10	$1/N_g$	1
s	cm	1	100	$1/N_g$	10
L	cm	1	250	$1/N_g$	25
D	cm	1	60	$1/N_g$	6
$\alpha = a/s$	%	1	10	1	10
H_{LTP}/s	%	1	0,4	1	0,4

Table 2. 3D RIs and scale factors at $N_g \times g$ =10×g.

parameters	unit	prototype		model	
H_{LTP}	cm	1	40	$1/N_g$	4
$\varnothing$	cm	1	12	$1/N_g$	1,2
s	cm	1	50	$1/N_g$	5
l	cm	1	50	$1/N_g$	5
D	cm	1	60	$1/N_g$	6
$\alpha = \pi\varnothing^2 / 4s^2$	%	1	4,52	1	4,52
H_{LTP}/s	%	1	0,8	1	0,8

2.2 2D rolling load

The rolling load consists of an outer steel tube$^{(1)}$ with a diameter *of* D = 6 cm, length L = 25 cm, inside which two smaller tubes can slide (figure 4a): $D^{(2)}$ = 4 cm and $D^{(3)}$ = 2 cm, with respective masses M = 2.9 kg; 1.8 kg and 0.6 kg to simulate possible variable loads (tubes$^{(1) \text{ or } (1+2) \text{ or } (1+2+3)}$). The travel speed of the mobile gantry pushing the wheel is 25 cm/min (figure 4b).

2.3 3D Rolling Load

The model load is a wheel consisting of a short, thick steel tube with a mass of m = 0,6 kg, a width *of* l = 5 cm and an outer diameter *of* D = 6 cm. The travel speed of the mobile gantry that pushes the wheel is always 25 cm per minute (figure 6a). A highly flexible 0.5 mm thick polyvinyl chloride (PVC) film placed on the LTP prevents the wheel from sinking into the sand during back and forth movements, and is a negligible reinforcement. Both the roller and the wheel are positioned on the PVC film before the centrifugal acceleration phase.

In order to model one-way traffic (figure 6b), an electromagnet with a capacity of 1800 N was fixed under the mobile gantry, to magnetically suspend the roller or wheel after each one way trip, and then bring the load back to its starting point.

2.4 Instrumentation

The nine 2D RIs, all along the container, are made of rigid aluminum plates fixed on a thick aluminum plate that simulates the bedrock (figures 2 and 5.a). The RIs are all recessed at the foot. These RIs measure a=1 cm in thickness and L=25 cm in length, in model scale.

They are arranged every s = 10 cm. Three RIs in the middle of the model (RI1, RI2, RI3) are instrumented with two vertical force sensors fixed between their toe and the bedrock.

The forty five 3D aluminium RIs with a diameter ∅ = 12 mm are embedded at the foot in the same bedrock (figure 5b, five transverse mesh lines). A vertical force sensor is attached between the toes of seven RIs and the bedrock whose positions are shown in figure 3.

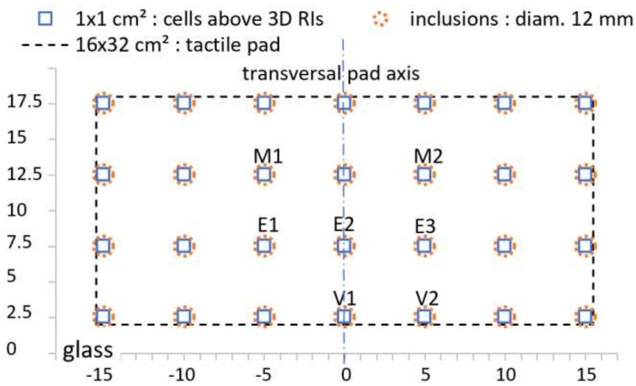

Figure 3. RIs(3D) under the tactile pad; 7 instrumented RIs

The vertical stress on the polystyrene layer $\sigma_{v(poly)}$ is measured using a flexible tactile pad (1 mm thick; 16 cm wide; 32 cm long) (TactArray, PPS Company©), consisting of 16 × 32 touch cells of 1 cm² (figure 7a), with a resolution of 0.021 kPa over a full measurement range of 69.8 kPa.

Two configurations, one with a tactile pad and the other without, were tested to ensure that the pad did not introduce reinforcement. By precisely placing the tactile pad, a transverse line of cells can then cover the 2D RIs (figure 7a), and similarly, a measuring cell can cover each of the 3D RI heads (figure 7b).

Two laser displacement sensors (Baumer©), mounted on the mobile gantry, measure vertical displacements at each end of the roller (figure 2). These sensors have an accuracy of ±0.1 mm.

Image analysis (acA4112-8gm/gc, Basler©) to evaluate maximum surface shear strains was conducted using GeoPIV-RG software (Stanier et al., 2016). In parallel, Picture software (Moliard, 1993) was used to monitor sand displacements and GGR sheet tensioning, based on the trajectories of visual markers located behind the container window. Each marker consists of a tip affixed to the geogrid edge (figure 7c) and a head coated with grease to maintain contact with the front glass (figure 7d). Only the roll-induced displacements of the GGR with the 2D RIs in the following §.3.2 will be analyzed in this paper.

2.5 Materials

Under real-world conditions, the short duration of rolling loads compared to consolidation times means that clay soils exhibit unconsolidated and undrained behavior, and thus a quasi-elastic deformation response.

In the test models, this behaviour is simulated using an expanded monolith polystyrene (product Th.38, Knauf©), with a density of 15.5 kg/m³ and an E_{poly} modulus of elasticity equal to 1 MPa, determined by the oedometer. Its yield strength is about 80 kPa, which ensures that the rolling load at the service limit state Q will not cause it to puncture.

The polystyrene is carefully installed in the model in 2 layers of 2 cm thick with precise centering and diameter of the reservation holes to minimize friction with the RIs. Thanks to its near-zero Poisson ratio, compressed polystyrene transmits virtually no lateral stress. As a result, the vertical load Q_p at the top of the RIs is equal to the force measured by the vertical sensor minus the self-weight of the RI.

The LTP consists of a medium-dense Fontainebleau sand NE 34 (d_{50} = 0.21 mm) with a density index of I_d=0.73, implemented by sand raining. Its density is 1648 kg/m³ and the friction angle equals to 41 degrees (Dano et al., 2024).

The GGR (Windhager©) fiberglass is placed halfway up the LTP, and covers the entire surface of the container (Figure 7d). The ends of the GGR are free. It has a square mesh of 1.6 mm on each side and a thickness of 0.4 mm. With a tensile strength of 10 kN/m at 1% deformation, it offers a high stiffness J_{GGR} of 1 MN/m at model scale. In accordance with the scaling laws, Table 3 summarizes the correspondence between the material properties and the weight of the wheel. As a reminder, the stresses in the centrifugal model and those in the prototype are identical in order to reproduce identical internal frictions.

Table 3. Loading and materials characteristics

Materials & ELS Loading	**unit**	**Prototype**		**Model**	
ρ_d	kg/m³	1	1648	1	1648
J_{GGR}	N/m	1	10^7	$1/N_g$	10^6
E_u=E_{poly}	Pa	1	10^6	1	10^6
Q_{wheel}	N	1	5890	$1/N_g^2$	58.9
Q_{roller}	N	1	28450	$1/N_g^2$	284.5

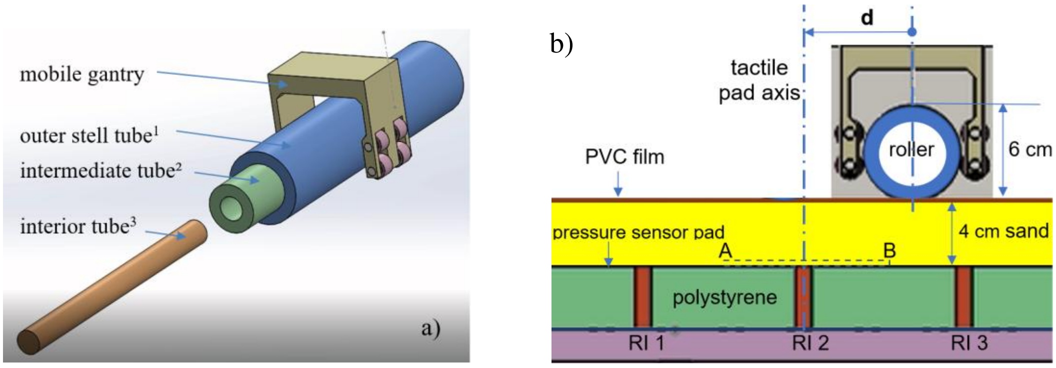

Figure 4. a) 3 nesting tubes form the rolling load; b) cross-section of the 2D RIs model; mobile gantry; mesh A-B

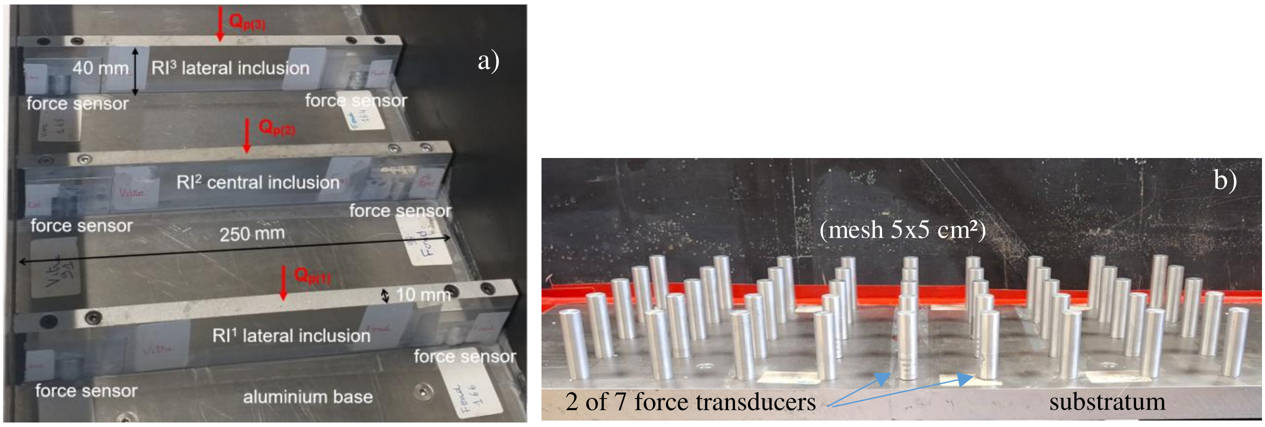

Figure 5. a) 3 of the 2D RIs instrumented with 2 vertical force transducers; b) network of 45 3D RIs, 7 are instrumented

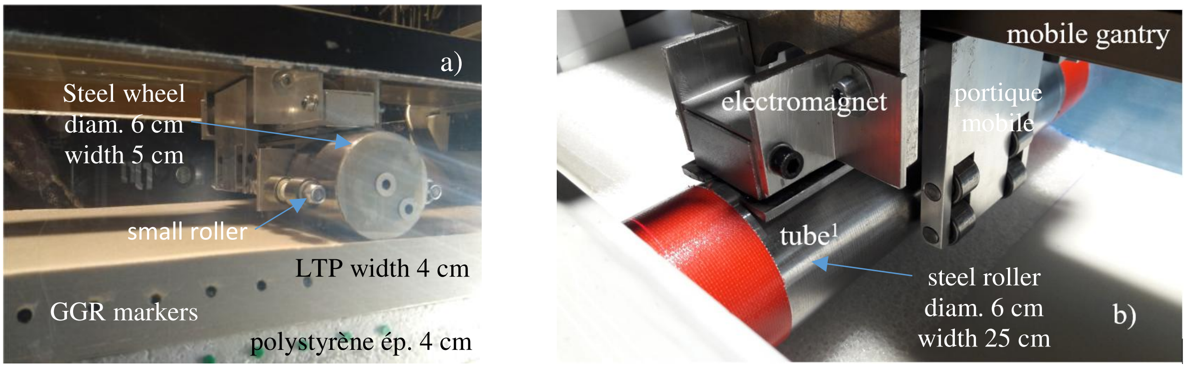

Figure 6. a) 3D wheel just behind the glass; b) 2D roller under the electromagnet (for one-way trips).

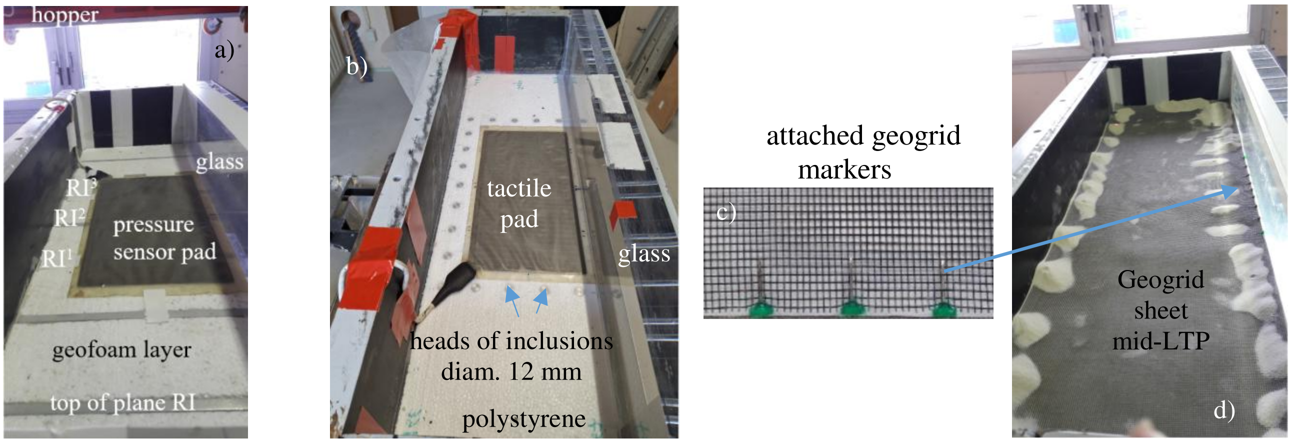

Figure 7. Tactile pad before rainfall: a) on 2D RIs, b) on 3D RIs; c) GGR markers; d) placement of the GGR at mid-LTP.

3 TEST RESULTS AND ANALYSIS

3.1 Some test results for the roller

The following are some recent test results with the heavy roller traffic only. Three models are analyzed: one model with RIs(2D) and GGR, a second with the same RIs(2D) without GGR, and a third with RIs(3D) without GGR (Table 4). We will study the tensioning of the GGR in the first one, and in the next two, the vertical stress under the LTP and the forces at the heads of the RIs.

Table 4. Programm of roller testing

Loading	**Roller**		
traffic	3 go and 2 return (3×G + 2×R)		
RIs	2D (plates)		3D (cylinder)
geogrid	with GGR	without GGR	
parameters studied	tensioning the GGR sheet at 1st passage	Vertical stress under the LTP and effort at the head of RIs during 5th passage	

3.2 Tensioning the geogrid sheet for RIs(2D)

The progressive tensioning of the GGR sheet is examined during the first Go, using the positions of nine markers attached to the GGR (numbered from 0 to 8, Figure 8). The roller moves from right to left.

The minimal anchorage length L_a at the roller departure is about equal to 25 cm. In reference, the available anchoring force, without vertical diffusion of roller load downstream, is evaluated in model scale at: $\frac{1}{2}H_{LTP}\times B\times L_a\times N_g\times \rho\times g\times \tan\phi \approx 180$ N.

The relative elongations ($\Delta L_{i\text{-}j}/L_{i\text{-}j(o)}$) of four successive adjacent sections are plotted in figure 9: $L_{0\text{-}2}$; $L_{2\text{-}4}$; $L_{4\text{-}6}$ and $L_{6\text{-}8}$, calculated using the "Picture" image analysis. These elongations are expressed as a function of the relative position of the roller in relation to RI^1, RI^2 and RI^3, whose positions are indicated. The sections whose elongation is measured are represented by the segments $L_{i\text{-}j}$ on the horizontal axis.

It should be noted that these relative elongations are unchanged in the prototype scale.

The head force of the RI² reaches $Q_p = 16$ daN when the roller passes over it (Dubreucq and Thorel, 2025).

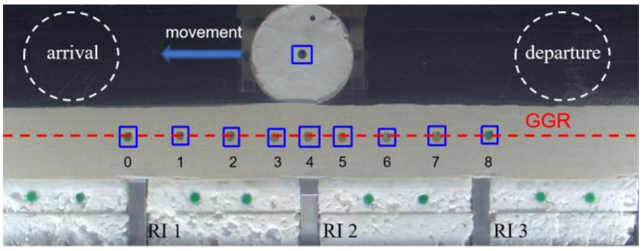

Figure 8. LTP with GGR, markers locations, 1stGo for roller

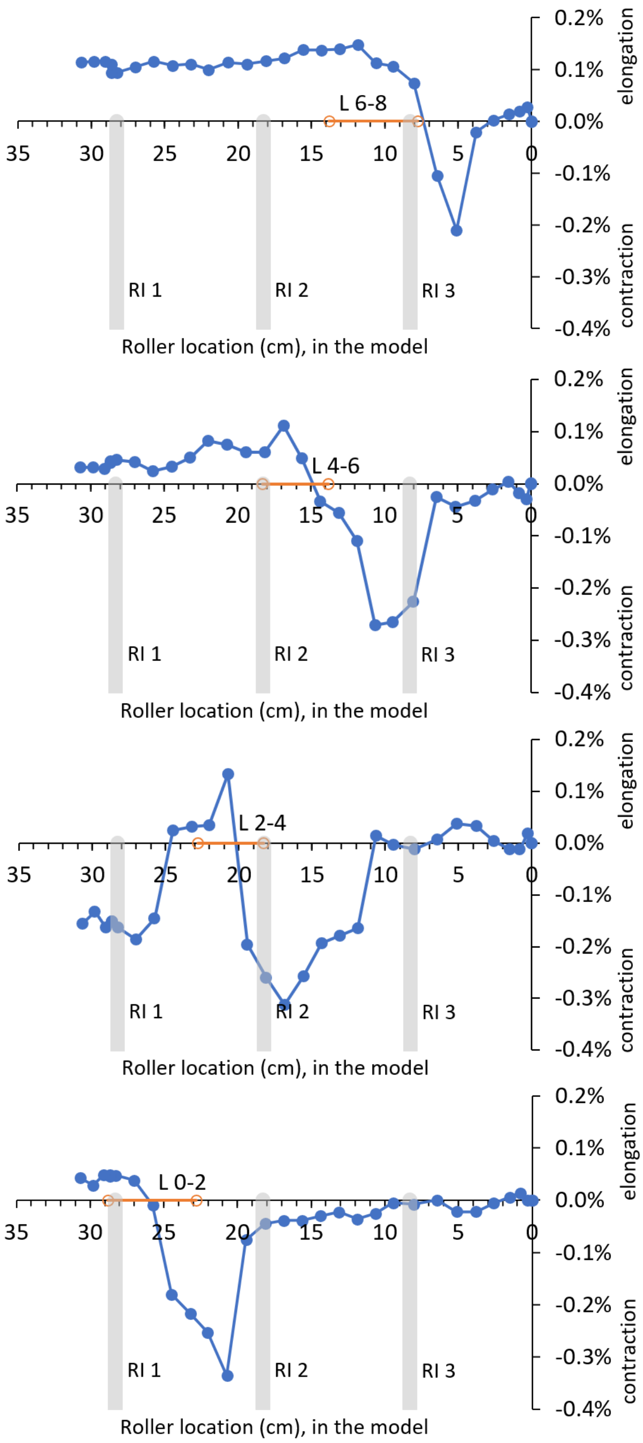

Figure 9. GGR relative contraction/elongation (blue line) in successive adjacent sections (orange line)

As the roller-tube[1] is in motion, the four GGR sections between RI1 and RI3 shorten by approximately -0.3%, then elongate shortly before the roller passes. Elongation is greatest when the roller is vertical to the left of the sections middle of the sections. The stretching then tapers off slightly, except for section $L_{2\text{-}4}$ downstream of RI², which eventually shortens. The average elongation is +0.05%, a very low value due to the high stiffness of the GGR. The associated tensile stress, $J_{GGR}\times\varepsilon_{GGR}\times L$, in the GGR is thus estimated : 125 N (i.e 12500 N in prototype).

3.3 Vertical stress at the base of the LTP

The tactile pad measured vertical pressures at the LTP base during the fifth pass, after 2 Go and 2 Return, above RI2(2D) (figure 10.a) and 5×RIs2(3D) (figure 10.b). *The 5th RIs(3D) longitudinal line is not covered*. The soil uplift after former passages explains the depressions above RI1 and RI3, or 5xRIs1 among others (inverse Marston'effect, Dubreucq et al. 2022).

From right to left, the roller approaches the RI² or the 5×RI²s transversal line (d=s/4), then positions itself above it (d=0) and passes to the other side (d=-s/4).

The stress calculated on soft soil without arching effect is: $q_{LTP}=\rho_d\times N_g\times g\times H_{TPC} = 6{,}5$ kPa.

As the roller approaches RI² or 5×RI²s, the pressure distribution is *completely* truncated upstream of RI² or 5×RI²s : part of the load is directly transferred to the top of RI² or 5×RI²s. Due to soil settlement which induces vertical force concentration on RIs (Marston's effect), sensor cell line (1 cm wide) closed to the right of RI2 or RIs2 less affected by the roller load. When the roller is above RI2 or 5×RIs2, load diffusion is concentrated at the top of RI2 or 5×RIs2, with a slightly adjacent transfer to the soft geofoam. The vertical pressure distribution then shifts symmetrically as soon as the roller passes over RI2 or 5×RIs2 which are slightly loaded, but not RI1 or 5×RIs1.

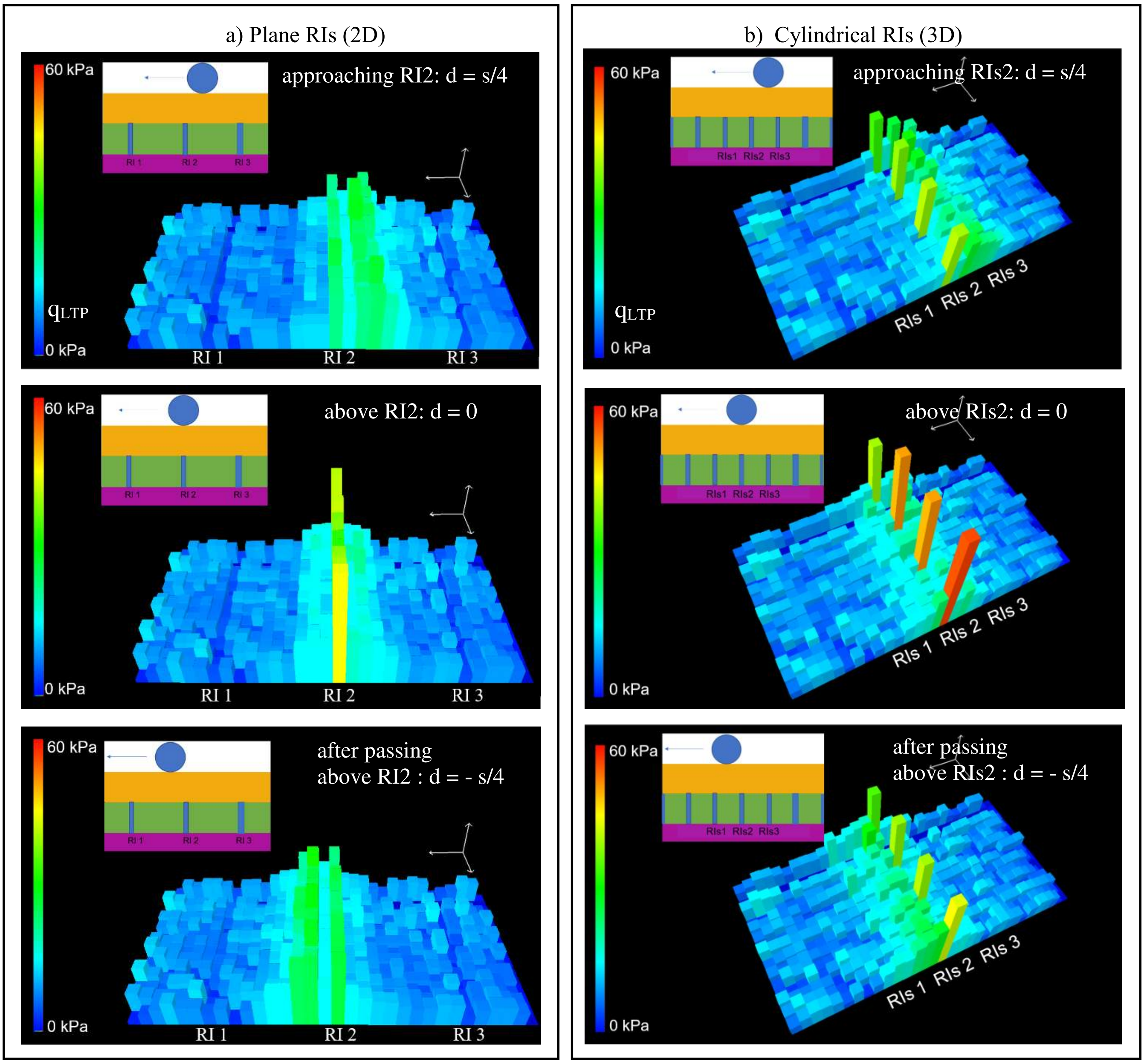

Figure 10. Pressure below LTP for the 5th roller pass : a) with RIs 2D (left figures); b) with RIs 3D (right figures); from top to bottom: approaching RI2 or 5xRIs2, above RI2 or 5xRIs2, after passing above RI2 or 5xRIs2

3.4 Load transfer efficiency for roller

The efficiency of load transfer E_Q to the RIs is analyzed over a distance of approximately 30 cm covered by the the roller at model scale (figure 4.b). E_Q varies with the reduced distance *d/s* between the roller axis and the RIs axis according to the equation:

$$E_{Q(d)} = \frac{\sum_{i=1}^{n} Q_{p(d)i}}{n \times W_{LTP} + (m/p) \times Q_{\text{roller}}} \qquad (1)$$

where $Q_{p(d)i}$ is the top force of the instrumented RI (i) ; W_{LTP}, the mesh weight: $q_{LTP} \times s \times L$ (2D), $q_{LTP} \times s^2$ (3D); *n,* the total number of these meshes (i); *p* (resp. *m*), the number of transverse (resp. instrumented) meshes.

2D RIs Case. During the 2nd return and the 3rd go, $Q_{p(d)}$ reaches 110 N in model scale (figure 11a), 31% lower than that obtained with GGR (see §.3.2). The $Q_{p(d)}$ curves are asymmetrical with an G/R offset equal to about $2 \times a$.

Before any rolling, $E_{(Q=0)}$ for 2D RIs is 0.16 on average over the three instrumented RIs.

As *d/s* varies from 0 to 0.5, Q_{roller} is transferred mostly to RI2 and little to RI3, allowing us to consider a double transfer cells, $2 \times W_{LTP}$, with m = p = 1 for 2D RIs.

Thus $E_{Q(d)}$ varies from about 0.02 (roller between RI2 et RI3), to 0.18 (roller above RI2) (figure 11b).

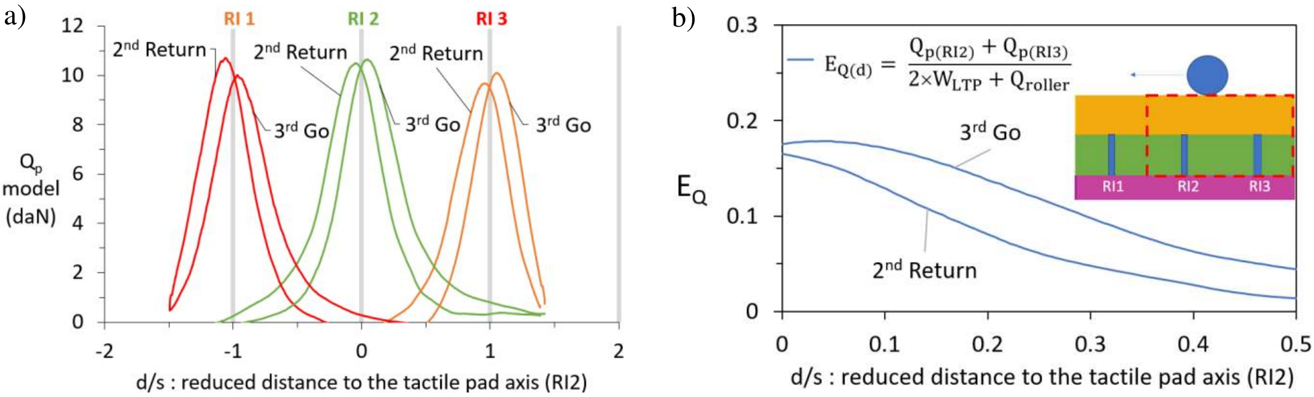

Figure 11. 2D RIs : a) head forces ; b) load RI2 efficiency, both depending on the roller location (no GGR)

3D RIs Case. The $Q_{p(d)}$ curves of the seven load cells are symmetrical, with a G/R peak offset equal to approximatively 2×∅ (figure 12a). Before first rolling, $E_{(Q=0)}$ for 3D RIs is 0.47 on average over the seven instrumented RIs. During rolling $Q_{p(d)(M2)}$ is about half the the forces measured on the two RIs, designated by E3 and V2 (figure 3), despite their location on the same transverse line: the model remains imperfect.

By symmetry, the force measured on E1 is adopted for E1', and the force E2 on E2'.

As *d/s* varies from 0 to 0.5, considering three out of five transverse cells, Q_{roller} is transferred in part to E2', E2, V1, and to a lesser extent to M2, E3 and V2, or even M1, E1 and E1' when *d/s* tends to 0 (figure 12b). Therefore $9 \times W_{LTP}$ and m=3 out of p=5 transverse meshes are retained in the $E_{Q(d)}$ efficiency calculation.

During the 2nd Return and the 3rd Go, $E_{Q(d)}$ varies from 0.2 in *d/s* = 0.5 between the transverse mesh lines 5×RIs2 and 5×RIs3, to 0.23 in *d/s* = 0 above the 5×RIs2 line.

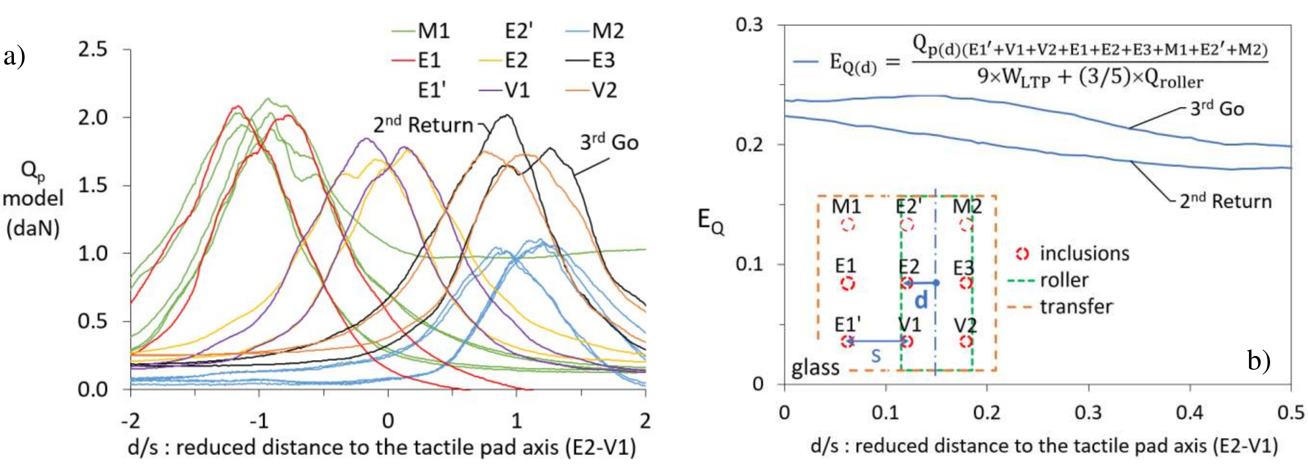

Figure 12. 3D RIs : a) head forces ; b) load efficiency, both depending on the roller location (no GGR).

4 CONCLUSIONS

In terms of rolling load traffic on soft soils reinforced by s-to-center RIs, original 2D and 3D models were carried out in a centrifuge in a transparent-faced container. The granular load transfer plateform has a low relative thickness in 2 D ($H_{LTP}/s = 0.4$; $\alpha = 10\%$.) to medium in 3D ($H_{LTP}/s = 0.8$; $\alpha = 4.52\%$), reinforced by a possible GGR of high stiffness. The RIs are all recessed at their toes in the substratum. Tests at the serviceability limit state simulate linear traffic of a prototype roller (weight: 2845 daN, diameter: 60 cm, length: 250 cm) in round-trips. The progressive tensioning of the GGR is quantified.

In the model without the GGR, depending on the position of the roller in relation to the RIs, the E_Q load transfer efficiency varies between 18 and 23% to the 3D RIs, and between 2 and 18% to the 2D RIs : a sufficient H_{LTP}/s relative thickness and 3D RIs prevail.

The settlements and deformations in the LTP remain to be studied in detail by image analysis.

Ongoing tests are being carried on the traffic of a prototype wheel (weight: 589 daN, same diameter, width: 50 cm), above the 3D RIs, in round trips or one-way trips, with or without the GGR.

ACKNOWLEDGEMENTS

The French national project ASRI+ fund this work by a cooperative research project (managed by IREX) with the support of the Ecological Transition Ministry.

REFERENCES

AISRI (French National Research Project on Rigid Inclusions). (2013). Recommandations pour la conception, le calcul, l'exécution et le contrôle des ouvrages sur sols améliorés par inclusions rigides verticales, *IREX, Presses des Ponts,* Paris, France: https://asiriplus.fr/

Briançon L, Thorel L, Simon B. (2021). ASIRI+: French National Research Program on soil Reinforcement with Rigid Inclusions. *4th Int. Conf. Transport. Geotech. (ICTG)* Chicago, Illinois, USA Aug.30-Sept. 2. Postponed 24-27 may 2021. *Proc. Adv. Transp. Geotech. IV*, Lecture Notes in Civil Eng. 2020.165, paper 462. 6p. https://doi.org/10.1007/978-3-030-77234-5_54.

Dano C, Thorel L, Dupla J-C, Benahmed N, Li Z. (2024). Compilation des propriétés physiques et mécaniques du sable de Fontainebleau NE34. *Revue Française de Geotechnique*, 179, 6. https://doi.org/10.1051/geotech/2024027.

Dubreucq T.,Thorel L., Jagu A.,Lerat L., Alain Neel A.,Gaudicheau P., Audrain P.(2022), 2D effect of static or rolling load on a granular platform above a soft soil reinforced by rigid inclusions, *10th ICPMG 2022,* Daejeon, Korea, hal-04073349

Dubreucq T.,Thorel L. (2025). Low thickness platform on soft soil reinforced with rigid inclusions: 2D rolling load tests in centrifuge, *Transportation Geotechnics* 56 (2026) 101800, https://doi.org/10.1016/j.trgeo.2025.101800

Garnier J. Physical models in geotechnics: state of the art and recent advances, in: *First Coulomb Lecture* (*Caquot Conference*, 3rd October, Paris). 2001; 1–51. https://doi.org/10.1051/geotech/2020003.

Liu K, Xu S, Wen M, Feng W, Zhang Z, Wan Z, (2025). Investigation on load sharing ratio of piles and soil in GRPS embankment with different pile types and geogrid layers under long-term cyclic loading, *Transp. Geotechnics* 51 (2025) 101534. https://doi.org/10.1016/j.trgeo.2025.101534

Lukiantchuki J A, OliveRIa J R M S, Pessin J, Almeida M S. (2018) Centrifuge modelling of traffic simulation on a construction waste layer. *Int. J. Phys. Mod. in Geotechnics;* 18(6): 290–300. https://doi.org/10.1680/jphmg.17.00012.

Marston A, Anderson A O. (1913) The theory of loads on pipes in ditches and tests of cement and clay drain tile and sewer pipes. *Engineering Experiment Station Bulletin*, Iowa State College, 1913; 31.

Moliard J M. (1993) Logiciel Picture: Outil de traitement d'images appliqué aux essais en centrifugeuse. *Rapport LCPC*; 54p.

Stanier S, Blaber J, Take W, White D. (2016) Improved image-based deformation measurement for geotechnical applications. *Can. Geotech*. J.; 53 (5), 727-739. https://doi.org/10.1139/cgj-2015-0253.

Thorel L, Baudoin G, Rault G, Derkx F, Buttigies S. (2007). Modélisation en centrifugeuse du renforcement de sols compressibles par inclusions rigides : dispositifs du transfert de charge par cisaillement. *Congrès Français de Mécanique*, Grenoble, France. hal-03358168.

Van Eekelen S J M, Han J. (2020) Geosynthetic-reinforced pile-supported embankments: state of the art. *Geosynthetics International*. 2020; 112–141. https://doi.org/10.1680/jgein.20.00005.

Wu P, Chen W, Feng W, Yin J, Ho T, Huang S. (2024) Load transfer mechanism of geotextile-reinforced sand layer over semrigid column-improved soft soil. *Acta Geotechnica* 19:2855–2871. https://doi.org/10.1007/s11440-023-02213-8